# Dynamics of a single electron in the disordered Holstein model

F.X. Bronold
*Institut für Theoretische Physik, Otto-von-Guericke-Universität Magdeburg*
*Universitätsplatz 2, PF 4120, 39016 Magdeburg, Germany*

A. Saxena and A.R. Bishop
*Theoretical Division and Center for Nonlinear Studies, Los Alamos National Laboratory,*
*Los Alamos, New Mexico 87545*



We study, at zero temperature, the dynamics of a single electron in a Holstein model augmented by site-diagonal, binary-alloy type disorder. The average over the phonon vacuum and the alloy configurations is performed within a generalized dynamical coherent potential approximation. We present numerical results for a Bethe lattice with infinite coordination number. In particular, we investigate, in the intermediate electron-phonon coupling regime, the spectral and diffusion properties in the vicinity of the high-energy edge of the lowest polaronic subband. To characterize the diffusion properties, we define a spectrally resolved delocalization time, which is, for a given energy, the characteristic time scale on which the electron leaves a given site. We find the delocalization times substantially enhanced for states with a large phonon content, i.e., in the absence (presence) of alloy-type disorder at the high-energy edge(s) of the polaronic subband (mini-subbands). According to their delocalization times, we discriminate between "fast" *quasi-particle-like* and "sluggish" *defect-like* polaron states and qualitatively address the issue of trapping of an electronic carrier.

PACS numbers: 71.38.+i, 72.10.Di, 71.35.Aa

## I. INTRODUCTION

In nature there is an abundance of "polaronic" compounds in which, due to strong electron-phonon coupling, electrons and phonons lose, in a certain temperature and density range, their individual identity and new entities emerge: polarons [1]. Examples of current interest are, among others, the high-temperature superconducting perovskites [2], the "colossal" magneto-resistance manganites [3], and the titanates [4]. The details of the actual materials notwithstanding, it is commonly assumed that, at least qualitatively, many aspects of these compounds can be understood on the basis of the Holstein model [5] supplemented by various terms, such as, e.g., Coulomb repulsion, spin-orbit coupling, and specific forms of material imperfections.

In its basic form the Holstein model comprises a single tight-binding band locally coupled to dispersionless optical phonons. Despite this simplicity, the properties of the Holstein model are not yet fully understood. Even in the extreme dilute limit, that is the case of a single polaron in an otherwise empty band, many basic questions remain, despite impressive theoretical progress made in recent years [6–13].

In particular, the notoriously difficult issue of trapping [10–13] is far from being completely resolved. The trapping properties are only understood for the polaron *groundstate* of the ordered Holstein model. In an important paper, Löwen [10] has rigorously shown that the groundstate of the ordered Holstein model has to be itinerant, thereby implying that the groundstate can be only trapped by an *external* process, e.g., driven by material imperfections. Although it is not clear whether Löwen's proof also applies to *excited* states of the polaron, it is generally assumed that *all* states in the ordered Holstein model are itinerant. Hence, if trapping occurs, it has to be externally driven. Indeed, translational invariance of the Holstein model seems to force all (eigen)states to be itinerant. On the other hand, the non-existence of translational invariance does not necessarily prohibit itinerant states. For a single electron in a random potential, for example, itinerant states exist, separated from localized states by a "mobility edge", despite the absence of translational invariance. Likewise, as noted above, translational invariance per se might be no guarantee that all polaron states are itinerant. That is, the important question about the trapping properties of *excited* polaron states is essentially unanswered.

Evidently, the broad theoretical task is to construct a rigorous "mobility-edge-theory" for *excited* polaron states, treating extrinsic and (possibly) intrinsic trapping processes on an equal footing. In view of the complexity of this problem, we are not yet able to develop such a rigorous theory. Instead, we present in this paper, as a first step, an approximate investigation of the spectral and diffusion properties of that part of the spectrum, where we expect a rigorous theory to predict a mobility edge. In particular, we investigate, in the intermediate electron-phonon coupling regime and with an approximate technique, the states comprising the high-energy edge of the lowest polaronic subband. The dispersion is extremely flat in this part of the spectrum indicating, perhaps, already the tendency of (intrinsic) trapping. Definitely, very small amounts of disorder suffice to drive these states into the trapped regime.

Our investigation is based on the Holstein model augmented by site-diagonal, binary-alloy type disorder. Measuring energy in units of $2J$, where $J$ denotes

the electronic (nearest-neighbor) hopping integral, the Hamiltonian for the "Holstein alloy" reads in the single-electron sector

$$H = \epsilon_B \sum_i |i><i| - \frac{1}{2}\sum_{<ij>} |i><j| + \delta \sum_i x_i |i><i| + \Omega \sum_i b_i^\dagger b_i - g\sum_i (b_i + b_i^\dagger)|i><i|. \quad (1)$$

Here, $|i>$ stands for the Wannier state on site $i$ and $b_i[b_i^\dagger]$ annihilates [creates] an optical phonon on site $i$. The phonon frequency and the electron-phonon coupling constant (in units of $2J$) are denoted by $\Omega$ and $g$, respectively. Depending on the occupancy of the site, the on-site energy (in units of $2J$) is either $\epsilon_A$ or $\epsilon_B$. The scattering strength $\delta = \epsilon_A - \epsilon_B$ can be taken as a measure of the disorder. The independent random variables $x_i$ are drawn from a bi-modal probability distribution $p(x_i) = c\delta(x_i) + (1-c)\delta(x_i - 1)$, with $0 \le c \le 1$ ($c$ denotes the concentration of the B sites).

Spectral properties of the model, such as the density of states, the self-energy, and the spectral function, can be deduced from the electronic two-point function, which at temperature $T = 0$ and in Wannier representation reads

$$\mathcal{G}_{ij}(z) =< i|\bar{G}(z)|j >, \quad (2)$$

with an *averaged* one-resolvent

$$\bar{G}(z) = \langle\langle (0|G(z)|0)\rangle\rangle. \quad (3)$$

Here, $G(z) = 1/(z - H)$ denotes the one-resolvent and $\langle\langle ...\rangle\rangle$ and $(0|...|0)$ stand, respectively, for averages over the quenched disorder and the phonon vacuum. Henceforth, the term "averaged" implies, if not otherwise specified, averaged over both quenched disorder and the phonon vacuum.

From the spectral properties alone it is, in general, not possible to decide whether the states involved are itinerant (extended) or trapped (localized). A more reliable method to discriminate between the two kinds of states is to investigate the return probability $P$, i.e., the probability to find (in the long time limit) the electron on the same site at which it was initially injected. This criterion has been used, for example, to characterize electronic states in a random potential [14]. At $T = 0$ and in Wannier representation, the correlation function, whose long time limit is the return probability, reads

$$P(t) = \langle\langle (0| < i|e^{iHt}|i >< i|e^{-iHt}|i > |0)\rangle\rangle. \quad (4)$$

Using Abel's theorem, $P$ can be conveniently expressed in terms of $p(2\eta)$, the Laplace transform of $1/2P(t/2)$ [14]. Explicitly,

$$\begin{aligned} P &= \lim_{t\to\infty} P(t) \\ &= \lim_{\eta\to 0} 2\eta p(2\eta) \\ &= \lim_{\eta\to 0} 2\eta \int_{-\infty}^{\infty} \frac{d\omega}{2\pi} f(\omega - i\eta, \omega + i\eta), \end{aligned} \quad (5)$$

where we have defined a four-point function

$$f(z_1, z_2) =< i|\bar{K}(z_1, |i >< i|, z_2)|i >, \quad (6)$$

given in terms of an *averaged* two-resolvent, which (for an arbitrary electronic operator $O_e$) reads

$$\bar{K}(z_1, O_e, z_2) = \langle\langle (0|G(z_1)O_eG(z_2)|0)\rangle\rangle. \quad (7)$$

The behavior of the spectrally resolved return probability,

$$P(\omega, \eta) = 2\eta f(\omega - i\eta, \omega + i\eta), \quad (8)$$

in the limit $\eta \to 0$ allows one to distinguish trapped from itinerant states. In particular, for a trapped polaronic defect state, $\lim_{\eta\to 0} P(\omega, \eta)$ is finite, whereas for an itinerant polaronic quasi-particle state $\lim_{\eta\to 0} P(\omega, \eta)$ vanishes.

The exact calculation of the averaged one- and two-resolvents for the Holstein alloy is a rather formidable task, and, due to lack of rigorous mathematical methods, we are forced to adopt an effective single-site averaging procedure. Specifically, we employ a generalized dynamical coherent potential approximation (DCPA) [15–20], which is known to capture the essentials of the polaron formation process.

Unfortunately, within the DCPA, trapped polaron states cannot be unambiguously identified, because $\lim_{\eta\to 0} P(\omega, \eta)$ vanishes for *all* energies $\omega$. Thus, rigorously speaking, the DCPA predicts all polaron states to be itinerant. Nevertheless, it is possible to give a qualitative discussion of the trapping issue. In particular, an asymptotic analysis of $P(\omega, \eta)$ for *finite* $\eta$ allows to define a spectrally resolved delocalization time, which is the characteristic time scale on which, at a given energy, the electron leaves a given site. According to their delocalization times, it is then possibe to distinguish between "fast" *quasi-particle-like* and "sluggish", i.e., temporarily trapped, *defect-like* polaron states.

The organization of the rest of the paper is as follows. Section II contains a general description of the DCPA with details about the calculation of the two- and the four-point functions defined above. Section III specializes the DCPA formalism to the Bethe lattice with infinite coordination number and discusses representative numerical results for the spectral and diffusion properties, respectively. Mathematical details not essential for the structure of the paper are relegated to two appendices. Finally, we conclude in section IV with a summary of key results and open questions.

## II. DYNAMICAL COHERENT POTENTIAL APPROXIMATION

### A. Perspective

In contrast to a classical alloy, where an electron experiences only elastic impurity scattering, the electron in a Holstein alloy is subject to elastic impurity and inelastic phonon scattering. Both scattering processes might possibly trap the electron. It is therefore necessary to treat them simultaneously. In particular, averages over the phonon vacuum and the alloy configurations need to be performed on an equal footing.

A powerful tool to approximately perform these two averages is the effective single-site approximation, where one embeds an individual scatterer into an effective medium to be determined self-consistently by enforcing the scattering from a single scatterer to vanish on the average. The main advantage of this scheme is the non-perturbative treatment of on-site correlations. In particular, the non-perturbative treatment of on-site electron-phonon correlations is an essential in order to capture polaron formation. The main drawback, on the other hand, is the insufficient treatment of inter-site correlations. It is the latter which eventually makes $\lim_{\eta\to 0} P(\omega,\eta)$ to vanish for all energies $\omega$, irrespective of the model parameters, and, thus, prevents a rigorous calculation of diffusion and trapping properties. However, as indicated in the Introduction, an asymptotic analysis of $P(\omega,\eta)$ for finite $\eta$ partly compensates for this shortcoming.

In the case of elastic impurity scattering the effective single-site approximation yields the well-known coherent potential approximation (CPA) [21–23]. The DCPA, originally developed by Sumi [15], is a direct extension of the CPA to problems involving *inelastic* scattering. It has been primarily used to investigate linear [15,16] and nonlinear [17–19] optical properties of polaron-excitons in molecular crystals. However, it can be applied to any on-site inelastic scattering process. Paquet and Leroux-Hugon [20] employed the DCPA, e.g., to investigate a single quantum particle subject to an on-site potential which fluctuates in time according to discrete or continuous Markov processes.

The CPA as well as the DCPA are mean field approximations for a single electron subject to impurity or phonon scattering, respectively. The most general mean field approximation, applicable also to dense quantum systems with mutual inelastic scattering between its constituents, is the dynamical mean field approximation (DMFA) [24–26]. [Naturally, in the limit of a single electron, interacting with a bath (of phonons or random scatterers), the DMFA reduces to the (D)CPA.] It can be shown, assuming that the nearest-neighbor hopping integral is scaled by a factor $1/\sqrt{Z}$, where $Z$ denotes the coordination number of the lattice, that the DMFA provides an *exact* solution of the original model in the limit of $Z \to \infty$. Accordingly, the DMFA [i.e., in the respective limits, the (D)CPA] can be either considered as an exact theory for lattices with $Z = \infty$ or as an approximate theory for lattices with finite $Z$.

The DMFA has been employed by Ciuchi et al. [11] to study, in various electron-phonon coupling regimes, the groundstate and the spectral properties of a single electron in the *ordered* Holstein model. As indicated above, for a single electron, the DMFA reduces to the DCPA. The investigations of Sumi and Ciuchi et al. are therefore closely related.

Postponing to section III a discussion of how our investigation complements the DCPA work by Sumi [15] and the DMFA work by Ciuchi et al. [11], we shall now present a derivation of the generalized DCPA formalism as needed to determine two-point and four-point functions for the Holstein alloy.

### B. Calculation of $\bar{G}(z)$

In the spirit of the CPA we introduce an effective medium described by an effective one-resolvent

$$G_{eff}(z) = \frac{1}{z - H_{eff}(z)}, \tag{9}$$

with

$$H_{eff}(z) = H_B + \Sigma(z), \tag{10}$$

and

$$H_B = \epsilon_B \sum_i |i><i| - \frac{1}{2} \sum_{<ij>} |i><j| + \Omega \sum_i b_i^\dagger b_i. \tag{11}$$

The unknown energy-dependent coherent potential (self-energy) operator $\Sigma(z)$ defined with respect to the reference Hamiltonian $H_B$ will be specified by enforcing a self-consistency condition, namely the averaged one-resolvent is forced to be equal to the averaged effective one-resolvent, i.e.,

$$\bar{G}(z) = (0|G_{eff}(z)|0), \tag{12}$$

where we have used the configuration independence of $G_{eff}(z)$.

In the above equations, the energy variable $z$ denotes the *total* energy of the coupled electron-phonon system and not just the electron energy. The coherent potential seen by the electron, on the other hand, depends of course only on the electron energy. Therefore, the energy argument of the coherent potential is the total energy $z$ minus the lattice energy, which is, neglecting the zero point motion of the phonons, just the total number of phonons in the system times the phonon frequency. A convenient way to ensure that the coherent potential is only a function of the electron energy is to define, following ref. [20],

a set of projection operators $P_q$, which project onto the phonon subspace with a total number of $q$ phonons, and to write for the coherent potential operator

$$\begin{aligned}\Sigma(z) &= \sum_q \sum_i P_q \Sigma_i^{(q)}(z) \\ &= \sum_q \sum_i P_q v^{(q)}(z) |i><i|, \end{aligned} \tag{13}$$

with $v^{(q)}(z) = v(z - q\Omega)$. From now on we shall adopt the convention that any operator or function with a superscript $(q)$ has to be taken at the energy $z - q\Omega$. Note, in accordance with the spirit of the CPA, that the coherent potential $v(z)$ does not contain any spatial information: It neither depends on the site nor on the spatial distribution of the excited phonons.

Combining this ansatz for $\Sigma(z)$ with Eq. (9), we obtain for the effective one-resolvent

$$G_{eff}(z) = \sum_q P_q g^{(q)}(z), \tag{14}$$

with auxiliary (electronic) operators

$$g^{(q)}(z) = \frac{1}{z - q\Omega - \sum_{\vec{k}} [\epsilon_B + \epsilon_{\vec{k}} + v^{(q)}(z)] |\vec{k}><\vec{k}|}. \tag{15}$$

Apparently, in contrast to the full one-resolvent $G(z)$, the effective one-resolvent $G_{eff}(z)$ is a simple operator in the phonon Hilbert space. For an arbitrary phonon state $|\{n_l\})$

$$G_{eff}(z) |\{n_l\}) = g^{(\sum_l n_l)}(z) |\{n_l\}) \tag{16}$$

holds, i.e., (phonon) subspaces with different total phonon number are decoupled and, as a consequence, the self-consistency condition Eq. (12) becomes

$$\bar{G}(z) = g^{(0)}(z). \tag{17}$$

In order to derive a functional equation for the unknown function $v(z)$, which in turn specifies $\bar{G}(z)$, we perform a multiple-scattering analysis in the product Hilbert space of the coupled electron-phonon system. Except for the underlying Hilbert space, the mathematical manipulations parallel the CPA multiple-scattering analysis of ref. [22]. The basic relation between the full and effective one-resolvents,

$$G(z) = G_{eff}(z) + G_{eff}(z) T(z) G_{eff}(z), \tag{18}$$

involves the total T-matrix,

$$T(z) = \sum_i Q_i(z), \tag{19}$$

which, according to ref. [22], can be expressed in terms of individual single-site contributions

$$Q_i(z) = t_i(z) \left[ 1 + G_{eff}(z) \sum_{j \neq i} Q_j(z) \right], \tag{20}$$

with the atomic T-matrix given by

$$t_i(z) = \left[ 1 - \Delta H_i(z) G_{eff}(z) \right]^{-1} \Delta H_i(z). \tag{21}$$

From Eq. (20) we see that $Q_i(z)$ is a product of the atomic T-matrices $t_i(z)$ and an effective wave factor $\left[ 1 + G_{eff}(z) \sum_{j \neq i} Q_j(z) \right]$ describing an effective wave incident on site $i$ modified by multiple-scattering events. The single-site perturbation

$$\begin{aligned}\Delta H_i(z) = &\left[ \delta x_i - g \left( b_i^\dagger + b_i \right) - \sum_q P_q v^{(q)}(z) \right] \\ &\times |i><i| \end{aligned} \tag{22}$$

comprises bi-modal alloy type fluctuations and coupling to localized phonons on site $i$.

Combining Eq. (18) with Eq.(19) and taking Eq. (16) into account, the self-consistency condition Eq. (17) is satisfied if we enforce

$$\langle\langle (0|Q_i(z)|0) \rangle\rangle = 0. \tag{23}$$

Iteration of Eq. (23) gives rise to an intractable infinite series involving *all* sites of the lattice. The standard procedure to obtain a numerically feasible description is to factorize the average in Eq. (23) into a product of averages, i.e., to average atomic T-matrices and effective wave factors separately. Relegating a discussion of the factorization procedure to the next subsection, we approximate Eq. (23) by

$$\begin{aligned}\langle\langle (0|Q_i(z)|0) \rangle\rangle \approx &\langle\langle (0|t_i(z)|0) \rangle\rangle \\ &\times \langle\langle (0|1 + G_{eff}(z) \sum_{j \neq i} Q_j(z)|0) \rangle\rangle, \end{aligned} \tag{24}$$

reducing thereby the self-consistency condition to $\langle\langle (0|t_i(z)|0) \rangle\rangle = 0$. Because phonons on sites $j \neq i$ are not affected by scattering events encoded in $t_i(z)$ (they are "frozen" and act only as "spectators"), the single-site self-consistency condition can be formulated more generally as

$$\begin{aligned}\langle\langle (N, 0_i|t_i(z)|0_i, N) \rangle\rangle &= \langle\langle (0, 0_i|t_i^{(N)}(z)|0_i, 0) \rangle\rangle \\ &= 0 \quad \forall \quad N, \end{aligned} \tag{25}$$

where $|n_i, N)$ denotes an arbitrary phonon state with $n$ phonons on site $i$ and a total number of $N$ phonons on all the other sites. Note the usage of the supersript notation defined above. The physical interpretation of Eq. (25) is the following: The electron "remembers" how many virtual phonons it has excited in previous scattering events (and, accordingly, how much energy is stored in the lattice); it does not "remember", however, at which sites these events took place.

Instead of working directly with Eq. (25), it is more convenient to introduce an equivalent polaron-impurity model (PIM) [18], which describes a single perturbation $\Delta H_i(z)$ self-consistently embedded into an effective medium. Mathematically, the PIM is formulated by

$$D_i(z) = G_{eff}(z) + G_{eff}(z)t_i(z)G_{eff}(z) \quad (26)$$
$$= G_{eff}(z) + G_{eff}(z)\Delta H_i(z)D_i(z). \quad (27)$$

The self-consistency equation (25) is then transformed into

$$\langle\langle(0,0_i|D_i^{(N)}(z)|0_i,0)\rangle\rangle = g^{(N)}(z), \quad (28)$$

which in turn yields for the averaged one-resolvent

$$\bar{G}(z) = g^{(0)}(z) = \langle\langle(0,0_i|D_i(z)|0_i,0)\rangle\rangle. \quad (29)$$

As shown in appendix A, it is straighforward to derive from the PIM a non-linear functional equation for the local two-point function. We get

$$\mathcal{G}_{ii}(z) = \frac{1-c}{[F^{A,(0)}(z)]^{-1} - \dfrac{g^2}{[F^{A,(1)}(z)]^{-1} - \dfrac{2g^2}{[F^{A,(2)}(z)]^{-1} - }}} + \frac{c}{[F^{B,(0)}(z)]^{-1} - \dfrac{g^2}{[F^{B,(1)}(z)]^{-1} - \dfrac{2g^2}{[F^{B,(2)}(z)]^{-1} - }}} \quad (30)$$

with

$$F^{\lambda,(n)}(z) = \frac{1}{z - n\Omega - \epsilon_\lambda + \mathcal{G}_{ii}^{-1}(z-n\Omega) - \mathcal{R}[\mathcal{G}_{ii}(z-n\Omega)]}, \quad (31)$$

where $\mathcal{R}[\xi]$ denotes the inverse Hilbert transform (see below).

For $c = 0$ Eqs. (30)–(31) have been given before by Sumi [15] and independently by Ciuchi et al. [11]. Various limits of the $c = 0$ equations, e.g., weak, intermediate, and strong electron-phonon coupling limits, have been discussed in these references. The non-linear functional couples local two-point functions with energies shifted by any *negative* integer multiple of $\Omega$. This accounts for the fact that at zero temperature only phonon emission is possible. At finite temperature, in contrast, absorption of thermally excited phonons is also allowed. In that case, local two-point functions with energies shifted by *any* integer multiple of $\Omega$, negative as well as positive, would be coupled [11,15].

The coherent potential $v(z)$ can be directly obtained from Eq. (29). Specifically, introducing the Hilbert transform $\mathcal{H}[\xi]$ corresponding to the bare density of states $N_0(E) = (1/N)\sum_{\vec{k}} \delta(E - \epsilon_{\vec{k}})$, the local two-point function can be written as

$$\mathcal{G}_{ii}(z) = \int dE \frac{N_0(E)}{z - \epsilon_B - v^{(0)}(z) - E} = \mathcal{H}[z - \epsilon_B - v^{(0)}(z)]. \quad (32)$$

Employing the inverse Hilbert transform, defined by $\mathcal{R} * \mathcal{H}[\xi] = \xi$, finally leads to

$$v^{(0)}(z) = z - \epsilon_B - \mathcal{R}[\mathcal{G}_{ii}(z)]. \quad (33)$$

The local two-point function $\mathcal{G}_{ii}(z)$ uniquely determines the coherent potential $v^{(0)}(z)$. Once $v^{(0)}(z)$ is known any matrix element of the averaged one-resolvent can be obtained.

### C. Validity of the Factorization Procedure

In the previous subsection we employed a factorization procedure to reduce the multi-site self-consistency condition to a single-site condition. Clearly, the mathematically exaxt average of the operator $Q_i$ contains many terms which are not zero, even if the atomic T-matrix vanishes. The single-site self-consistency condition can be only approximate. We now analyze the validity of the factorization procedure taking advantage of the connection between the DCPA and the DMFA. As a by-product, we shall find an efficient way to derive the DCPA equations for the averaged two-resolvent.

To that end, we follow ref. [27] and rearrange the multiple-scattering series into clusters containing a fixed number $p$ of lattice sites. We write (suppressing the energy variable $z$)

$$Q_i = \sum_p Q_i^{[p]} \quad (34)$$

with $Q_i^{[1]} = t_i$ and

$$Q_i^{[p]} = t_i \sum_{j_1 \neq i} G_{eff} t_{j_1}^{[2]}(i) \sum_{j_2 \neq i, j_1} G_{eff} t_{j_2}^{[3]}(i, j_1) \; ... \sum_{j_{p-1} \neq i, j_1, ..., j_{p-2}} G_{eff} t_{j_{p-1}}^{[p]}(i, j_1, ..., j_{p-2}) \quad (35)$$

for $p \geq 2$. The cluster T-matrices $t_{j_{p-1}}^{[p]}(i, j_1, ..., j_{p-2})$ are defined as the sum of all scattering processes involving at most $p$ *different* sites $i, j_1, ..., j_{p-1}$ with the constraint that the entrance site has to be $j_{p-1}$. This constraint ensures that all p sites contributing to $Q_i^{[p]}$ are connected. The exit site, on the other hand, can be any site of the p-cluster. Notice that, in contrast to the original multiple-scattering series given in Eq. (20), where only successive summation indices had to be different, *all* summation indices in Eq. (35) are different.

We are now in a position to evaluate the importance of each individual multiple-scattering term contributing to $Q_i$. Keeping in mind that all processes where a site

$j$ is visited only once vanish due to the single-site self-consistency condition Eq. (25), only processes where *all* sites are *at least* visited twice require further analysis. Figure 1 schematically depicts the first non-vanishing $p = 2$ process (i.e., a fourth order process in which each of the two sites is visited twice). Writing

$$t_{nm}^{(r)} =< i|(0, n_i|t_i^{(r)}|m_i, 0)|i > \tag{36}$$

for the (configuration dependent) matrix elements of the atomic T-matrix, this process is analytically given by

$$Q_i^{[2],4^{th}} = \sum_{j\neq i,qr} t_{0r}^{(0)} \mathcal{G}_{ij}^{(r)} t_{0q}^{(r)} \mathcal{G}_{ji}^{(r+q)} t_{r0}^{(q)} \mathcal{G}_{ij}^{(q)} t_{q0}^{(0)} |i >< j|. \tag{37}$$

To proceed further, we now imagine at this point that the hopping matrix element is scaled by $1/\sqrt{Z}$ (as in the case of the DMFA). Then, we immediately see that for large $Z$ Eq. (37) is at least $\sim 1/\sqrt{Z}$ because it contains three off-diagonal two-point functions and only one free summation over sites $j$, i.e., for $Z \to \infty$ this process does not contribute to $Q_i$ at all. In fact, it can be shown that all p-cluster processes in which *all* $p$ sites are at least visited twice are suppressed by a factor containing the inverse of the coordination number $Z$. As a consequence, for $Z \to \infty$ these processes vanish and need not be explicitly considered in the averaging procedure.

The implication of the above discussion is three-fold. First, it corroborates, using multiple-scattering theory, the conventional CPA technique, previous work by Vlaming and Vollhardt [28], who showed, acknowledging earlier work by Schwartz and Siggia [29], that for a lattice with infinite coordination number any CPA-type theory becomes exact, i.e., for infinite coordination number, the single-site self-consistency condition is indeed sufficient to ensure that the average of $Q_i$ as a whole vanishes.

Second, it indicates that even for a finite coordination number, processes which do not vanish due to the single-site self-consistency condition are at least suppressed.

Third, from a formal point of view, the DCPA is equivalent to the replacement of the full operator $Q_i$ by a reduced operator $Q_i^{SAP}$ containing only *self-avoiding paths* (SAP); $Q_i^{SAP}$ can be obtained from Eq. (35) by setting $t_{j_{p-1}}^{[p]}(i, j_1, ..., j_{p-2}) = t_{j_{p-1}} \forall\ p$. The coherent potential $v(z)$ is then adjusted in such a way that the averaged $Q_i^{SAP}$ vanishes. This procedure can be envisaged, in physical terms, as a *loss of spatial memory*, because the electron "assumes" that each site it encounters is visited the first time, i.e., the electron does not "remember" whether it has visited the site before. Naturally, for a lattice with infinite coordination number, this is exact, because the probability that the electron returns to the same lattice site is vanishingly small.

The replacement $Q_i \to Q_i^{SAP}$, i.e., the erasur of the spatial memory of the electron, is of course consistent with the ansatz for the (local) self-energy operator. On the other hand, this replacement leads to an insufficient treatment of inter-site processes in the calculation of the averaged two-resolvent and, eventually, prevents a rigorous calculation of the diffusion and trapping properties.

Keeping this shortcoming in mind, we shall nevertheless employ this formal replacement from the outset in the next subsection to simplify the calculation of the four-point function.

### D. Calculation of $\bar{K}(z_1, O_e, z_2)$

The discussion of the previous subsection suggests that the single-site self-consistency condition is, from a formal point of view, equivalent to the replacement $Q_i \to Q_i^{SAP}$, i.e., only SAPs need to be explicitly considered in the averaging procedure. We now show that this replacement allows a rather straightforward derivation of the averaged two-resolvent.

For that purpose, we first recast Eq. (7), using Eqs. (16) and (18) together with the self-consistency condition, Eq. (25), into

$$\bar{K}(z_1, O_e, z_2) = g^{(0)}(z_1) \left[O_e + \bar{\Gamma}(z_1, O_e, z_2)\right] \times g^{(0)}(z_2). \tag{38}$$

Keeping only site-diagonal terms, the electronic vertex operator is given by

$$\bar{\Gamma}(z_1, O_e, z_2) = \sum_i \langle\langle (0|\Gamma_i(z_1, O_e, z_2)|0)\rangle\rangle, \tag{39}$$

with a local vertex operator

$$\Gamma_i(z_1, O_e, z_2) = Q_i^{SAP}(z_1) G_{eff}(z_1) O_e G_{eff}(z_2) \tilde{Q}_i^{SAP}(z_2). \tag{40}$$

In the above equations we have kept only retraceable SAP's where the second leg of the path, encoded in $\tilde{Q}_i^{SAP}$, retraces in *reversed* order the first leg of the path, encoded in $Q_i^{SAP}$ and neglected retraceable SAP's where the second leg retraces the first leg in the *same* order. In more familiar terms (see Fig. 2), we have kept the ladder diagrams and neglected (maximally) crossed diagrams. This choice is consistent with the coherent potential determined in the previous subsection. In particular, it can be shown that the local vertex defined in the ladder approximation and the local self-energy obey the Ward identity corresponding to particle conservation [23].

In analogy with the classical alloy problem, we expect the maximally crossed diagrams to yield a significant (for certain model parameters possibly diverging) contribution to the local vertex function. As a consequence, a consistent treatment of these processes might render the potential to force $\lim_{\eta\to 0} P(\omega, \eta)$ to be finite for some energies $\omega$ and for certain model parameters. Accordingly, itinerant and trapped polaron states could be rigorously distinguished. We did not, however, succeed in taking them into account.

To derive an explicit equation for the local vertex function (in the ladder approximation), we have to perform the average of Eq. (40). To that end, it is advantageous to derive a formal operator equation for the local vertex operator $\Gamma_i$. For simplicity, we shall from now on suppress the arguments of the various operators. The implied arguments should be clear from the context. If we visualize Eq. (40) in terms of diagrams (see Fig. 3), we readily obtain

$$\Gamma_i = t_i G_{eff} \left[ O_e + \sum_{j \neq i} \Gamma_j^{(-i)} \right] G_{eff} t_i, \tag{41}$$

where $\Gamma_j^{(-i)}$ stands for the vertex operator on site $j$ given by summing up all "ladder-type paths" not visiting site $i$. Consequently, as far as the configuration average is concerned, the atomic T-matrices $t_i$ and the term between the brackets are statistically independent and the configuration average factorizes, i.e.,

$$\langle\langle \Gamma_i \rangle\rangle = \langle\langle t_i G_{eff} \langle\langle \left[ O_e + \sum_{j \neq i} \Gamma_j^{(-i)} \right] \rangle\rangle G_{eff} t_i \rangle\rangle. \tag{42}$$

For a macroscopic solid we expect $\langle\langle \Gamma_j^{(-i)} \rangle\rangle$ essentially to be the same operator as $\langle\langle \Gamma_j \rangle\rangle$. Hence, if we dealt only with alloy-type disorder, Eq. (42) would be the result given by Velický [23]. To cope with inelastic scattering, we have to keep in mind, however, that the vertex function (similar to the coherent potential) depends only on the electron energy, i.e., we have to keep track of the energy stored in the lattice (given by the total number of virtual phonons). Consistent with the ansatz for the local self-energy operator, we therefore write

$$\begin{aligned} \langle\langle \Gamma_i \rangle\rangle &= \sum_q P_q \Gamma_i^{(q)} \\ &= \sum_q P_q \gamma_i^{(q)} |i><i|, \end{aligned} \tag{43}$$

with $\gamma_i^{(q)} = \gamma_i(z_1 - q\Omega, O_e, z_2 - q\Omega)$. Thus, the phonon vacuum expectation value of Eq. (42) becomes

$$\gamma_i^{(0)} = \langle\langle \sum_q t_{0q}^{(0)} \left[ K_i^{(q)} - \mathcal{G}_{ii}^{(q)} \gamma_i^{(q)} \mathcal{G}_{ii}^{(q)} \right] t_{q0}^{(0)} \rangle\rangle, \tag{44}$$

with

$$K_i^{(q)} = < i | g^{(q)} O_e g^{(q)} | i > + \sum_l \mathcal{G}_{il}^{(q)} \gamma_l^{(q)} \mathcal{G}_{li}^{(q)}. \tag{45}$$

Note, the only configuration dependent quantities are now the matrix elements of the atomic T-matrix.

The linear functional for the vertex function is not "local" in the energy variables $z_1$ and $z_2$. Instead, due to the possibility of phonon emission, Eq. (44) couples all vertex functions with energies shifted by any *negative* integer multiple of $\Omega$.

Employing spatial Fourier transforms,

$$K_{\vec{Q}}^{(r)} = \sum_i e^{-i\vec{Q}\cdot\vec{R}_i} K_i^{(r)}, \tag{46}$$

$$a_{\vec{Q}}^{(r)} = \sum_i e^{-i\vec{Q}\cdot\vec{R}_i} < i | g^{(r)} O_e g^{(r)} | i >, \tag{47}$$

$$\mathcal{A}_{\vec{Q}}^{(r)} = \sum_{\vec{R}_i - \vec{R}_j} e^{-i\vec{Q}\cdot[\vec{R}_i - \vec{R}_j]} \mathcal{G}_{ij}^{(r)} \mathcal{G}_{ji}^{(r)}, \tag{48}$$

$$\gamma_{\vec{Q}}^{(r)} = \sum_i e^{-i\vec{Q}\cdot\vec{R}_i} \gamma_i^{(r)}, \tag{49}$$

it is straigthforward to combine Eqs. (44) and (45) and to derive, after some rearrangements, a single equation for the Fourier-transformed local vertex function:

$$\begin{aligned} \gamma_{\vec{Q}}^{(0)} = & \sum_q \langle\langle t_{0q}^{(0)} t_{q0}^{(0)} \rangle\rangle a_{\vec{Q}}^{(q)} \\ & + \sum_q \langle\langle t_{0q}^{(0)} t_{q0}^{(0)} \rangle\rangle \{ \mathcal{A}_{\vec{Q}}^{(q)} - \mathcal{G}_{ii}^{(q)} \mathcal{G}_{ii}^{(q)} \} \gamma_{\vec{Q}}^{(q)}. \end{aligned} \tag{50}$$

This equation reduces in the limit $\Omega = 0$ to Velický's vertex equation [23] for a model with a Gaussian distribution of on-site energies on top of a bi-modal distribution of on-site energies. Note, moreover, that $\gamma_{\vec{Q}}^{(0)}$ may be used to calculate *any* matrix element of the averaged two-resolvent of interest, i.e., the averaged two-resolvent is completely determined by $\gamma_{\vec{Q}}^{(0)}$.

## III. NUMERICAL RESULTS FOR THE $Z = \infty$ BETHE LATTICE

### A. Final Set of Equations

In the previous section, we neither specified the coordination number $Z$ nor the structure of the underlying lattice. The DCPA equations for the one- and two-resolvents can be used for arbitrary lattices. On the other hand, we have shown in subsection II.C that the single-site factorization procedure essentially ignores processes, where the electron returns to the same lattice site. It is therefore consistent with the DCPA to use a lattice, which, by construction, completely prohibits this type of processes. A particularly simple case is the $Z = \infty$ Bethe lattice. (It should be emphasized, however, that, within the DCPA, the numerical results, in particular for the spectrally resolved return probability, are not affected much by the chosen lattice.)

The main simplification, as far as the calculation of the local two-point function is concerned, arises from the fact that the inverse Hilbert transform for a $Z = \infty$ Bethe lattice is an algebraic relation, namely $\mathcal{R}[\xi] = 1/4\xi + 1/\xi$, which makes the self-consistent solution of Eqs. (30)–(31) particularly easy.

The calculation of the local vertex function simplifies even more, because, for a $Z = \infty$ lattice, Eq. (48) reduces (for almost all $\vec{Q}$) to $\mathcal{A}^{(r)}_{\vec{Q}}(z_1, z_2) \approx \mathcal{G}^{(r)}_{ii}(z_1)\mathcal{G}^{(r)}_{ii}(z_2)$ [26]. Therefore, the second term on the rhs of Eq. (50) vanishes and the local vertex function becomes

$$\gamma^{(0)}_{\vec{Q}} = \sum_q \langle\langle t^{(0)}_{0q} t^{(0)}_{q0}\rangle\rangle a^{(q)}_{\vec{Q}}, \tag{51}$$

which yields for the Fourier transform of Eq. (45):

$$K^{(0)}_{\vec{Q}} = a^{(0)}_{\vec{Q}} + \mathcal{G}^{(0)}_{ii}\mathcal{G}^{(0)}_{ii} \sum_q \langle\langle t^{(0)}_{0q} t^{(0)}_{q0}\rangle\rangle a^{(q)}_{\vec{Q}}. \tag{52}$$

To investigate the trapping properties of the polaron states, we need the four-point function $f(z_1, z_2)$ defined in Eq. (6). To that end, we set $O_e = |i><i|$ in the above equation and obtain after Fourier transformation

$$f(z_1, z_2) = \mathcal{G}_{ii}(z_1)\mathcal{G}_{ii}(z_2) + \mathcal{G}_{ii}(z_1)\mathcal{G}_{ii}(z_2) \times \sum_q \langle\langle t^{(0)}_{0q}(z_1) t^{(0)}_{q0}(z_2)\rangle\rangle \mathcal{G}^{(q)}_{ii}(z_1)\mathcal{G}^{(q)}_{ii}(z_2). \tag{53}$$

This equation holds for any lattice with $Z = \infty$. The structure of the lattice, i.e., in our case, the structure of the Bethe lattice, enters only through the local two-point function $\mathcal{G}_{ii}(z)$.

In appendix B we show that Eq. (53) can be brought into a form which allows us to calculate $f(\omega - i\eta, \omega + i\eta)$ from the amplitudes $\mathcal{D}^{\lambda,(0)}_{r0}(\omega + i\eta)$ defined in appendix A. Specifically,

$$f(\omega - i\eta, \omega + i\eta) = (1 - c)\sum_{r=0}^{\infty} |\mathcal{D}^{A,(0)}_{r0}(\omega + i\eta)|^2 + c\sum_{r=0}^{\infty} |\mathcal{D}^{B,(0)}_{r0}(\omega + i\eta)|^2, \tag{54}$$

i.e., the calculation of the four-point function $f(\omega - i\eta, \omega + i\eta)$ requires the same (moderate) numerical effort as the calculation of the local two-point function $\mathcal{G}_{ii}(\omega + i\eta)$.

The numerical strategy is now as follows. First, we truncate the continued fraction expansions in Eq. (30) and find the fixed point $\mathcal{G}^{(fix)}_{ii}(\omega + i\eta)$ by iteration. The density of states then follows directly from

$$N(\omega) = -\frac{1}{\pi} Im \mathcal{G}^{(fix)}_{ii}(\omega + i\eta). \tag{55}$$

To study the individual contributions of the A and B sites, we also calculate the component density of states

$$N_\lambda(\omega) = -\frac{1}{\pi} Im \mathcal{D}^{\lambda,(0)}_{00}(\omega + i\eta). \tag{56}$$

The amplitudes $\mathcal{D}^{\lambda,(0)}_{00}$, which are also needed in the calculation of the spectrally resolved return probability (see below), are given by the first ($\lambda = A$) and the second ($\lambda = B$) term on the rhs of Eq. (30) without the factors $1 - c$ and $c$, respectively, and with $\mathcal{G}_{ii}(z) = \mathcal{G}^{(fix)}_{ii}(z)$.

Second, we insert $\mathcal{G}^{(fix)}_{ii}(\omega + i\eta)$ in Eq. (33) and obtain the coherent potential $v^{(0)}(\omega + i\eta)$, which yields, using Eqs. (15) and (17), the spectral function

$$A(\omega, \epsilon_{\vec{k}}) = -\frac{1}{\pi} Im \frac{1}{\omega + i\eta - \epsilon_B - \epsilon_{\vec{k}} - v^{(0)}(\omega + i\eta)}. \tag{57}$$

Third, to calculate the spectrally resolved return probability $P(\omega, \eta)$ defined in Eq. (8), we truncate the sums in Eq. (54) and successively construct the amplitudes $\mathcal{D}^{\lambda,(0)}_{r0}(\omega + i\eta)$ from the recursion relation, Eq. (A10), starting from $\mathcal{D}^{\lambda,(0)}_{00}(\omega + i\eta)$ with $\lambda = A, B$. The truncation procedures and the subsequent numerical solution of the truncated equations for small $\eta > 0$ converge very well.

### B. Spectral properties

In this subsection we discuss the spectral properties of a subclass of polaron states, which we expect to be very susceptible to an (intrinsic or extrinsic) trapping transition. However, as mentioned in the Introduction, spectral properties alone cannot be used, even within a rigorous theory, to decide whether states are itinerant or trapped.

We start with the ordered Holstein model [model (1) with $\delta = 0$], which is characterized by two parameters, $\lambda = 2g^2/\Omega$ and $\alpha = g/\Omega$. (Recall, we measure energy in units of $2J$.) These parameters are conventionally used to define strong, intermediate, and weak electron-phonon coupling regimes [30]. The overall DCPA spectral features of which have been thoroughly investigated by Ciuchi et al. [11] and by Sumi [15]. The most intriguing of these regimes is, perhaps, the intermediate electron-phonon coupling regime, approximately defined by $\lambda \geq 1$ and $\alpha \geq 1$, where a finite number of polaronic subbands starts to develop on the low energy side of the bare density of states. The formation of these polaronic subbands, in particular as a function of $\lambda$ and $\alpha$, has been intensively studied in above mentioned references. For our purpose, it is sufficient to focus, for a fixed $\lambda$ and $\alpha$, on the *lowest* polaronic subband.

Generic numerical results for the ordered Holstein model in the intermediate electron-phonon coupling regime are summarized in Fig. 4. The polaron parameters are given in Table I. We first focus on panels (a) and (b), which depict the density of states $N(\omega)$, the imaginary part of the coherent potential $Imv(\omega)$, and the spectral function $A(\omega, \epsilon_{\vec{k}})$, respectively. The spectrally resolved return probability $P(\omega, \eta)$ shown in panel (c) will be discussed in the next subsection.

The main spectral characteristics in the intermediate electron-phonon coupling regime is the formation of a well-established lowest polaronic subband with an

asymmetric, steeple-like density of states, separated from the rest of the spectrum by a hard gap. Below the phonon emission threshold, which is inside the second polaronic subband, no residual scattering takes place, i.e., $Imv(\omega) = 0$. That is, within the lowest polaronic subband, the electron and the phonons arrange themselves into a new (composite) entity – a polaronic quasi-particle [11]. [The pole of $Imv(\omega)$ slightly above the high-energy edge of the lowest polaronic subband does not imply a diverging scattering rate; it merely signals the presence of the gap.] That the *quasi-particle concept* indeed applies can be also seen from the spectral function, which features a (dispersive) quasi-particle peak in the energy range of the lowest polaronic subband. Notice the pronounced band flattening and the vanishing quasi-particle weight in the flat part of the dispersion. The band flattening is the reason for the steeple-like density of states. At higher energies a second quasi-particle peak corresponding to the second polaronic subband is visible until the point where it merges with the one-phonon scattering continuum.

Both the steeple-like shape of the density of states and the band flattening at the high-energy edge of the lowest polaronic subband are an *indirect* consequence of the pole in the imaginary part of the coherent potential. As can be seen in Figs. 5a and 5b, the pole in the imaginary part is accompanied by a divergence in the real part. [Both are broadened due to the finite value of $\eta$; the pole becomes a Lorentzian and the divergence becomes a pronounced kink.] The divergence, in turn, induces a pronounced energy dependence of $Rev(\omega)$ just below the high-energy edge and it is this strong energy dependence which, as we shall show below, eventually yields the steeple-like density of states and the band flattening. Physically, the energy dependence of the real part of the coherent potential reflects the increasing phonon admixture in the states as the high-energy edge of the subband is approached.

The discussion of the steeple-like subband density of states is facilitated by considering

$$N_{1^{st}}(\omega) = \frac{2}{\pi} Re \sqrt{1 - [\omega - \epsilon_B - Rev(\omega)]^2}, \qquad (58)$$

an exact analytical expression for the lowest subband density of states, which follows from Eqs. (55) and (32) in the limit $\eta \to 0$ and the fact that for the lowest subband $Imv(\omega) = 0$. Two conclusions can be drawn from Eq. (58). First, the position $\omega_m$ of the maximum of the subband density of states does not coincide with the high-energy edge $\omega_h$, because they are respectively given by $\omega_m - \epsilon_B - Rev(\omega_m) = 0$ (thin solid line in Fig. 5a) and $\omega_h - \epsilon_B - Rev(\omega_h) = 1$ (thin dashed line in Fig. 5a). Hence, the density of states at the high-energy egde is, albeit very step-like, not discontinuous, even for $\eta \to 0$. Second, Eq. (58) together with Figs. 5a and 5b reveal that the rapid change of $Rev(\omega)$ between $\omega_m$ and $\omega_h$, caused by the divergence *above* $\omega_h$, produces the rapidly dropping density of states in this particular energy range, and hence, the steeple-like shape.

Figures 5a and 5c suggest, moreover, that the rapidly changing $Rev(\omega)$ is also responsible for the band flattening. To be more specific, we recall that the dispersion $\omega(\epsilon_{\vec{k}})$ is given by the poles of the spectral function defined in Eq. (57). Therefore, the change of the dispersion with $\epsilon_{\vec{k}}$ becomes

$$\frac{d\omega(\epsilon_{\vec{k}})}{d\epsilon_{\vec{k}}} = (1 - \frac{dRev(\omega)}{d\omega}|_{\omega=\omega(\epsilon_{\vec{k}})})^{-1}, \qquad (59)$$

which is, of course, particularly small for $\omega_m \leq \omega \leq \omega_h$, since the divergence yields a large derivative of $Rev(\omega)$. It is, therefore, the *divergence-induced* strong $\omega$-dependence of the real part of the coherent potential which not only causes the steeple-like subband density of states but also the pronounced flattening of the subband dispersion.

The DCPA results for the lowest polaronic subband corroborate recently obtained direct numerical simulation results for a finite Holstein model in the single-electron sector [7–9]. Specifically, the band flattening and the vanishing quasi-particle weight in the flat part of the dispersion are in good qualitative agreement. Both effects, characteristic of the intermediate electron-phonon coupling regime, are manifestations of the strong on-site electron-phonon correlations, which yield an increasing phonon admixture in the states comprising the high-energy edge of the lowest polaronic subband [8].

Clearly, the phonon admixture in the states must significantly affect the diffusion properties. In particular, because the dispersion becomes extremely flat in the vicinity of the high-energy edge of the lowest polaronic subband, these states might be *temporarily* trapped. In the next subsection, we will present an analysis of the spectrally resolved return probability $P(\omega, \eta)$, which indeed shows that the high-energy edge states are extremely "sluggish".

However, first we illustrate the modifications of the lowest polaronic subband due to alloying. We expect disorder on the scale of the subband width to show the most dramatic effects and therefore restrict $\delta$ [in Eq. (1)] to small values. Further, to be specific, we chose the B atoms to be energetically close to the high-energy edge of the subbands, i.e., we consider $\delta < 0$.

Figure 6 shows representative numerical results for the Holstein alloy. The polaron parameters are the same as in Fig. 4 (see Table I) and the alloy parameters are $c = 0.5$ and $\delta = -0.01$. First, we focus again on panels (a) and (b), which summarize the spectral properties in the vicinity of the lowest polaronic subband. The spectrally resolved return probability shown in panel (c) will be discussed in the next subsection.

The main effect of alloying is the formation of two mini-subbands. For the chosen parameters both mini-subband density of states exhibit a pronounced asymmetric, steeple-like shape (see Fig. 6a). From the strong asymmetry of the component density of states, which are also depicted in Fig. 6a, we find, moreover, that, al-

though both A- and B-sites contribute almost equally to both mini-subbands, the steeple-like shape of the mini-subband density of states comes entirely either from the A-sites (lower mini-subband) or from the B-sites (upper mini-subband). As in the case without disorder, the steeple-like shape is due to strong on-site electron-phonon correlations, which yield a large phonon admixture in the states at the high-energy edges of the respective mini-subbands, and, as a consequence, to rather flat dispersions in these parts of the spectrum. The band flattening can be clearly seen from the spectral function shown in Fig. 6b.

The detailed appearance of the mini-subbands depends on the concentration $c$ and the scattering strength $\delta$. To indicate the concentration dependence, for example, we show in Fig. 7 the density of states $N(\omega)$ for a fixed scattering strength $\delta = -0.004$ and concentrations varying from the pure A crystal ($c = 0$) to the pure B crystal limit ($c = 1$). Note, first, the noticeable distortions of the density of states (at the high-energy edge) despite the fact that $\delta$ is much smaller than the polaronic subband width and, second, the lack of $c \leftrightarrow 1 - c$ symmetry. That rather small amounts of disorder suffice to restructure the high-energy edge can be also seen in Fig. 8, where the lower panel shows the density of states and the imaginary part of the coherent potential for $c = 0.5$ and three different scattering strengths $\delta$.

It is not necessary to present an exhaustive investigation of the alloying-induced spectral changes in the whole $c - \delta$ parameter plane. The data presented suffice already to show that the modifications of the lowest polaronic subband are very similar to the ones found in an AB alloy with an *artificial* steeple-like bare density of states [31]. Indeed, the broken $c \leftrightarrow 1 - c$ symmetry, the appearance of a B mini-subband at scattering strengths much smaller than the polaronic subband width, and the asymmetry between the component density of states have their counterparts in this artificial steeple alloy.

In the artificial steeple alloy, as well as in the Holstein alloy, states comprising the steeple-like structure in the density of states are very susceptible to impurity scattering. For the Holstein alloy this is intuitively clear, because the steeple in the density of states contains the states corresponding to the flat part of the dispersion. As indicated above, due to the large phonon admixture, these states might be temporarily trapped, which suggests that they feel the on-site, alloy-type disorder much more strongly than the other states. The discussion of the diffusion properties in the next subsection will substantiate this intuitive picture.

### C. Diffusion properties

The spectral properties in the vicinity of the high-energy edge of the lowest polaronic subband suggest that this part of the spectrum is very susceptible to an (intrinsic or extrinsic) trapping transition.

In the Introduction, we emphasized that the problem of trapping of a polaron should be methodologically addressed with the same techniques used to investigate the problem of localization of an electron in a random potential. In particular, we stressed that $\lim_{\eta\to 0} P(\omega, \eta)$ would be a rigorous criterion to distinguish itinerant polaronic quasi-particle states from (any) trapped polaronic defect states. We also pointed out, that a rigorous investigation of the trapping issue is unfortunately beyond the DCPA because, within the DCPA, $\lim_{\eta\to 0} P(\omega, \eta)$ vanishes for all energies $\omega$. Although trapped states cannot be unambiguously identified, it is possible to identify *temporarily* trapped states through the $\eta$-asymptotics of $P(\omega, \eta)$.

To motivate the investigation of the $\eta$-asymptotics of $P(\omega, \eta)$, we first emphasize that the spectrally resolved return probability $P(\omega, \eta)$ contains valuable information about the diffusion properties not only in the limit $\eta = 0$ (which is usually considered [14]) but also for a finite $\eta > 0$. For a correct interpretation of the data, we have to keep in mind, however, that a finite $\eta$ broadens all spectral features. In particular, the pole [divergence] in $Imv(\omega)$ [$Rev(\omega)$] becomes, as mentioned in the previous subsection, a Lorentzian [pronounced kink], smearing out the high-energy edges of the respective bands. A finite $\eta$ yields therefore small artificial tails extending into the gap regions. These tails have no direct physical meaning. In the following we analyze, therefore, the $\eta-$asymptotics of $P(\omega, \eta)$ only for energies $\omega$ below the respective sharp high-energy edges obtained for $\eta \to 0$ (see Fig. 5b and the insets of Figs. 9–11).

The physical content of $P(\omega, \eta)$ can be extracted from Figs. 4c, 5d, 6c, and the upper panel of Fig. 8, where we plot, for the model parameters given in the respective captions, $P(\omega, \eta)$ for $\eta = 10^{-4}$. All the data show that $P(\omega, \eta)$ does not uniformly (in $\omega$) approach zero as $\eta \to 0$. Instead, $P(\omega, \eta)$ is substantially enhanced for certain energies $\omega$. Close inspection of the data shows, moreover, that the maximum of $P(\omega, \eta)$ always occurs slightly below the high-energy edges of the respective (mini-)subbands, i.e., in the spectral regions where the dispersions become extremely flat. (This can be most clearly seen in Fig. 5.) The enhancement of $P(\omega, \eta)$ is caused by the band flattening and is therefore a direct measure of the sluggishness of the corresponding states due to their large phonon admixture. More precisely, because $1/\eta$ can be interpreted as a characteristic time scale, a large value of $P(\omega, \eta)$ implies that the electron in the state at energy $\omega$ is not yet delocalized on the time scale $1/\eta$. Thus, the $\eta-$asymptotics of $P(\omega, \eta)$, i.e., the way $P(\omega, \eta)$ approaches zero for $\eta \to 0$, reveals the time scale on which the state at energy $\omega$ is *temporarily* trapped. [Note, once more, we study the $\eta-$asymptotics of $P(\omega, \eta)$ only for $\omega$ below the $\eta \to 0$ high-energy edge and not for energies belonging to the artificial tail which is present for a finite $\eta$.]

In what follows we put these qualitative considerations on a mathematical basis. To that end, we first note that

Eq. (5) suggests to interpret $f(\omega - i\eta, \omega + i\eta)$ as a "spectral density" corresponding to $p(2\eta)$, the Laplace image of $1/2P(t/2)$. That is, $f(\omega - i\eta, \omega + i\eta)$ gives the *spectrally resolved* diffusion behavior of the electron in the $\eta$ domain. Accordingly, the counterpart of $f(\omega - i\eta, \omega + i\eta)$ in the time domain, which we denote by $F(\omega, t)$, is the "spectral density" corresponding to $1/2P(t/2)$. That is, it gives the *spectrally resolved* diffusion behavior of the electron in the time domain.

That the $\eta$-asymptotics of $P(\omega, \eta)$ indeed contain the spectrally resolved diffusion behavior of the electron can be clearly seen in Fig. 9, where, for the ordered Holstein model with the polaron parameters given in Table I, $P(\omega, \eta)$ is plotted as a function of $\eta$ for three representative energies $\omega$ within the lowest polaronic subband, i.e., for energies below the $\eta \to 0$ high-energy edge. For the Holstein alloy, the overall behavior of $P(\omega, \eta)$ is the same. All three curves feature a hump whose shape and position strongly depend on $\omega$. For $\omega$ in the immediate vicinity to the high-energy edge of the polaronic subband, the hump appears at a very small $\eta$ and is very sharp. Far inside the subband, in contrast, the maximum appears at a larger $\eta$ and is less pronounced. The distinct $\omega$ dependence of the hump indicates different charateristic time scales for the diffusion behavior of the respective states.

To explicitly extract this time scale, we perform an asymptotic expansion of $P(\omega, \eta)$ for small $\eta$. The data shown in Fig. 9 suggest making the following ansatz

$$P(\omega, \eta) \approx K(\omega) \frac{\frac{\eta}{\eta_0(\omega)}}{(1 + \frac{\eta}{\eta_0(\omega)})^{1+\nu(\omega)}}, \tag{60}$$

and determining the parameters $K(\omega)$, $\eta_0(\omega)$, and $\nu(\omega)$ through a least-square fit. The dashed lines in Fig. 9 show that this approach works reasonably well. Using the definition of $P(\omega, \eta)$ given in Eq. (8) and employing a general mathematical theorem about Laplace transforms [32], we obtain the asymptotic behavior of $F(\omega, t)$ for large $t$ [note, since we measure energy in units of $2J$, time is mearured in units of $(2J)^{-1}$]:

$$F(\omega, t) \approx K(\omega) \frac{(t\eta_0(\omega))^{\nu(\omega)}}{2\Gamma(1 + \nu(\omega))} e^{-t\eta_0(\omega)}, \tag{61}$$

where $\Gamma(x)$ denotes the Gamma function.

From this equation we infer that the parameter $\eta_0(\omega)$ gives rise to a characteristic time scale. Defining $T_0(\omega) = 1/\eta_0(\omega)$, we see, in particular, that for $t \gg T_0(\omega)$ the function $F(\omega, t)$ decays exponentially to zero. For $t \ll T_0(\omega)$, however, $F(\omega, t)$ is finite, implying that the state at energy $\omega$ is not yet delocalized. It is therefore natural to interprete $T_0(\omega)$ as a (spectrally resolved) *delocalization time* characterizing *temporary* trapping, i.e., $T_0(\omega)$ quantifies the "sluggishness" of the state at energy $\omega$.

In Fig. 10 we plot $T_0(\omega)$ for the ordered Holstein model in the vicinity of the high-energy edge of the lowest polaronic subband. The polaron parameters are the same as in Fig. 4 (see Table I). In the immediate vicinity of the high-energy edge, where the dispersion becomes extremely flat due to the high phonon admixture in the states, the delocalization times increase roughly three orders of magnitude (but do not diverge). That is, the states in the flat part of the polaronic subband appear to be temporarily trapped on the time scales where the rest of the states are already delocalized. Clearly, the band flattening and the enhanced delocalization times are correlated and have, moreover, the same microscopic origin, namely the increased phonon admixture in the states at the high-energy edge of the subband. More formally, it is the *divergence-induced* strong $\omega-$dependence of $Rev(\omega)$ for $\omega_m \leq \omega \leq \omega_h$ which causes the large delocalization times at the high-energy edge of the lowest polaronic subband.

At this point it is appropriate to comment on the work of Hotta and Takada [33] who suggested that for energies where the self-energy (or, in our case, the coherent potential) diverges, states would be trapped because of the infinitely strong electron-phonon coupling. They studied the half-filled (ordered) Holstein-Hubbard model, but their conclusion is quite general and should, if valid, hold for any model which produces divergences in the self-energy. Such divergences are, however, always inside a gap. In fact, they signal the presence of a gap, as can be seen, e.g., in Figs. 4 and 5, that is, there are no states at the divergence energy which could be trapped. In contrast, our investigation suggests that, it is the effect the divergence has on states *within* the spectrum, namely, the band flattening it causes below the high-energy edge of the lowest polaronic subband, which could perhaps induce trapping in that particular energy range. Within the DCPA, however, the effect is too weak, giving rise only to large but finite delocalization times and, hence, only to temporary trapping.

It has been also suggested [11] that, if, due to some mechanism, a finite density of states appears at the divergence energy, the corresponding states would be trapped. A finite $\eta$ simulates such a mechanism. However, as can be seen in Fig. 5, the maximum of $P(\omega, \eta)$ does not occur in the tail but roughly at the maximum of the subband density of states. Therefore, at least within the DCPA, it is the band flattening and *not* the tail which is responsible for large delocalization times.

The concept of the delocalization time provides an appealing explanation of the spectral changes induced by alloying. In the previous subsection we have seen that the high-energy edge of the polaronic subband responds much more strongly to alloying than the bottom of the subband. From the perspective of the delocalization time this is now clear, because the high-energy edge contains "sluggish" defect-like states, whose large delocalization times make them feel the randomness of the on-site potential particularly strongly.

The delocalization times are also modified due to alloying. This is shown in Fig. 11 for a particular set of alloy parameters, $c = 0.5$ and $\delta = -0.002$. The polaron

parameters are the same as before (see Table I). In the previous subsection we have seen that the main effect of alloying is the formation of two mini-subbands with, due to the large phonon admixture in the states, rather flat dispersions at the two high-energy edges. As a consequence, the delocalization times are now enhanced in two narrow energy regions: At the high-energy edge of the A mini-subband and at the high-energy edge of the B mini-subband. Note, as in the case without disorder, the enhancement of the delocalization times is due to the band flattening effect, i.e., it is driven by strong on-site electron-phonon correlations. Even with the assistance of electron-impurity scattering, the on-site correlations are however not strong enough to produce divergent delocalization times.

The numerical results for the delocalization times suggest that we may tentatively distinguish two types of states: "Fast" *quasi-partice-like* states and "sluggish" *defect-like* states. In the ordered Holstein model, defect-like states appear at the high-energy edge of the polaronic subband. Whereas in the Holstein alloy, defect-like states occur at the high-energy edges of the two mini-subbands. With and without disorder, strong on-site electron-phonon correlations are responsible for the formation of defect-like states. Because the delocalization times of the defect-like states are *several orders* of magnitude larger than the delocalization times of the quasi-particle-like states, it is moreover conceivable that the sluggishness of the defect-like states may anticipate the onset of trapping.

## IV. CONCLUSIONS

We have provided a self-contained description of the DCPA and employed it to investigate the dynamics of a single electron in the Holstein model augmented by site-diagonal, binary-alloy type disorder (Holstein alloy). Using multiple-scattering theory, the conventional CPA technique, we derived the DCPA equations for the averaged two- and four-point functions and emphasized the main approximation involved: namely, after each hop from one lattice site to another the electron's spatial memory is erased. We visualized the lack of spatial memory in terms of self-avoiding paths and employed this picture to give an intuitive explanation why the DCPA becomes exact for a system with infinite coordination number.

Our numerical results focused on the intermediate electron-phonon coupling regime, where polaronic subbands start to emerge. We investigated, for representative parameter sets, the effect of alloying on the high-energy edge of the lowest polaronic subband. These states are very susceptible to impurity scattering because of their large phonon admixture, which leads to a flat dispersion in this part of the spectrum, and, as a consequence, to a steeple-like density of states. The observed modifications of the spectral properties are therefore reminiscent of typical CPA results obtained for a model with a steeple-like density of states: A lack of $c \leftrightarrow 1-c$ symmetry, an appearance of mini-subbands in the vicinity of the steeple (i.e., high-energy edge) of the subband for scattering strengths much smaller than the subband width, and an asymmetry in the component density of states.

The most notable result is, however, the large enhancement of the spectrally resolved return probability $P(\omega, \eta)$ for small but finite $\eta$ in the narrow energy regions where the dispersion of the polaron states becomes extremely flat. This occurs in the absence (presence) of alloy-type disorder at the high-energy edge(s) of the polaronic subband (mini-subbands). To elucidate the physical meaning of this strong enhancement, we analyzed the $\eta-$asymptotics of $P(\omega, \eta)$ and introduced the concept of a spectrally resolved delocalization time which is the characteristic time scale on which, at a given energy, the electron leaves a given site. The strong enhancement of $P(\omega, \eta)$ in the flat part(s) of the subband (mini-subbands) signals large delocalization times. According to their delocalization times we could thus classify, within the limitations of the DCPA, "fast" quasi-particle-like polaron states at the bottom and "sluggish" defect-like polaron states at the top of the subband (mini-subbands).

Within the DCPA, we could not decide, however, whether "defect-like", i.e., temporarily trapped states are in fact "defect", i.e., trapped states. At this point it is important to recall that within the DCPA only on-site processes contribute to the delocalization times. In contrast, inter-site processes are completely neglected. Particularly, back-scattering processes are expected to have a significant effect. In the conventional alloy problem, for example, these processes even yield, depending on the model parameters, infinite delocalization times at certain energies. It is therefore conceivable that the DCPA results for the delocalization times of polaron states presented in this paper are only lower bounds and temporarily trapped states may in fact be trapped states. More sophisticated methods beyond the DCPA, taking back-scattering and other non-mean field effects explicitly into account, are clearly needed to further elucidate the trapping issue.

## ACKNOWLEDGMENTS

One of the authors (F.X.B.) would like to thank Prof. Dr. H. Böttger for several valuable discussions during the course of this work. Useful and stimulating conversations with Dr. Holger Fehske are also very much appreciated. F.X.B. also acknowledges the hospitality of the Theoretical Division at Los Alamos National Laboratory where this work was initiated. This work is supported in part by the U.S. Department of Energy.

## APPENDIX A: POLARON IMPURITY MODEL (PIM)

In this appendix we show how the local two-point function $\mathcal{G}_{ii}(z)$ can be calculated from the PIM. Towards that end, we apply $< i|(N, n_i|...|m_i, N)|i >$ on both sides of Eq. (27) and obtain in compact matrix notation

$$\begin{aligned}\mathcal{D}^{(N)}(z) &= \tilde{G}^{(N)}(z) + \tilde{G}^{(N)}(z) \\ &\times \left[\sigma_{imp}^{(N)}(x_i; z) + \sigma_{ph}^{(N)}(g)\right] \\ &\times \mathcal{D}^{(N)}(z),\end{aligned} \tag{A1}$$

with matrices

$$\mathcal{D}_{nm}^{(N)}(z) = < i|(0, n_i|D_i^{(N)}(z)|m_i, 0)|i >, \tag{A2}$$

$$\left[\sigma_{imp}^{(N)}(x_i; z)\right]_{nm} = \left[x_i\delta - v^{(N+n)}(z)\right]\delta_{n,m}, \tag{A3}$$

$$\left[\sigma_{ph}^{(N)}(g)\right]_{nm} = -g\sqrt{n+1}\delta_{m,n+1} - g\sqrt{n}\delta_{m,n-1}, \tag{A4}$$

$$\left[\tilde{G}^{(N)}(z)\right]_{nm} = \mathcal{G}_{ii}^{(N+n)}(z)\delta_{n,m}. \tag{A5}$$

To derive Eq. (A1) we employed $\Delta H_i(z) \sim |i >< i|$ together with $\mathcal{G}_{ii}^{(q)}(z) =< i|g^{(q)}(z)|i >$, which follows from the definition of $G_{eff}(z)$.

If we now introduce an auxiliary matrix

$$\tilde{H}^{(N)}(z) = \left[1 - \tilde{G}^{(N)}(z)\sigma_{ph}^{(N)}(g)\right]^{-1}\tilde{G}^{(N)}(z), \tag{A6}$$

which sums all electron-phonon scattering processes, Eq. (A1) can be rearranged into

$$\mathcal{D}^{(N)}(z) = \left[1 - \tilde{H}^{(N)}(z)\sigma_{imp}^{(N)}(x_i; z)\right]^{-1}\tilde{H}^{(N)}(z). \tag{A7}$$

The configuration average is straightforwardly performed since (single-site) randomness enters only through $\sigma_{imp}^{(N)}(x_i; z)$. We find, using the bi-modal probability distribution $p(x_i) = c\delta(x_i) + (1-c)\delta(x_i - 1)$,

$$\begin{aligned}\langle\langle\mathcal{D}^{(N)}(z)\rangle\rangle &= \int dx_i p(x_i)\mathcal{D}^{(N)}(z) \\ &= (1-c)\left[1 - \tilde{H}^{(N)}(z)\sigma_{imp}^{(N)}(1; z)\right]^{-1} \\ &\times \tilde{H}^{(N)}(z) \\ &+ c\left[1 - \tilde{H}^{(N)}(z)\sigma_{imp}^{(N)}(0; z)\right]^{-1} \\ &\times \tilde{H}^{(N)}(z) \\ &= (1-c)\mathcal{D}^{A,(N)}(z) + c\mathcal{D}^{B,(N)}(z),\end{aligned} \tag{A8}$$

or, explicitly in terms of matrix elements,

$$\langle\langle\mathcal{D}_{nm}^{(N)}(z)\rangle\rangle = (1-c)\mathcal{D}_{nm}^{A,(N)}(z) + c\mathcal{D}_{nm}^{B,(N)}(z), \tag{A9}$$

where the amplitudes $\mathcal{D}_{nm}^{\lambda,(N)}(z)$ satisfy a set of recursion relations ($\lambda = A, B$)

$$\begin{aligned}\mathcal{D}_{nm}^{\lambda,(N)}(z) &= F^{\lambda,(N+n)}(z)\delta_{n,m} - gF^{\lambda,(N+n)}(z) \\ &\times \left[\sqrt{n+1}\mathcal{D}_{n+1m}^{\lambda,(N)}(z) + \sqrt{n}\mathcal{D}_{n-1m}^{\lambda,(N)}(z)\right],\end{aligned} \tag{A10}$$

with

$$F^{\lambda,(n)}(z) = \frac{1}{z - n\Omega - \epsilon_\lambda + \mathcal{G}_{ii}^{-1}(z - n\Omega) - \mathcal{R}[\mathcal{G}_{ii}(z - n\Omega)]}. \tag{A11}$$

From the self-consistency condition, Eq. (29), finally follows

$$\begin{aligned}\mathcal{G}_{ii}(z) &= \langle\langle\mathcal{D}_{00}^{(0)}(z)\rangle\rangle \\ &= (1-c)\mathcal{D}_{00}^{A,(0)}(z) + c\mathcal{D}_{00}^{B,(0)}(z),\end{aligned} \tag{A12}$$

which directly yields Eq. (30) if the continued fraction expansion [34] for the amplitudes $\mathcal{D}_{00}^{\lambda,(0)}(z)$ is invoked to iteratively solve Eq. (A10).

## APPENDIX B: DERIVATION OF EQ. (54)

In this appendix, we bring Eq. (53) into the numerically more convenient form of Eq. (54). As a preparatory step we notice, using the definition of the PIM, Eq. (26), that the matrix elements of the atomic T-matrix defined in Eq. (36) can be written as

$$t_{0q}^{(0)}(z) = \frac{\mathcal{D}_{0q}^{(0)}(z) - \delta_{0q}\mathcal{G}_{ii}(z)}{\mathcal{G}_{ii}(z)\mathcal{G}_{ii}(z - q\Omega)}, \tag{B1}$$

with $\mathcal{D}_{0q}^{(0)}(z)$ defined in Eq. (A2); here, we employed again the identity $\mathcal{G}_{ii}^{(q)}(z) =< i|g^{(q)}(z)|i >$. If we now insert Eq. (B1) into Eq. (53) and take into account that $\langle\langle\mathcal{D}_{00}^{(0)}(z)\rangle\rangle = \mathcal{G}_{ii}(z)$, Eq. (53) reduces to

$$f(z_1, z_2) = \sum_{q=0}^{\infty}\langle\langle\mathcal{D}_{0q}^{(0)}(z_1)\mathcal{D}_{q0}^{(0)}(z_2)\rangle\rangle. \tag{B2}$$

For $z_1 = z_2^* = z^*$, we may use $v^{(0)}(z) = [v^{(0)}(z^*)]^*$ and slightly rearrange the above equation into

$$f(z^*, z) = \sum_{q=0}^{\infty}\langle\langle|\mathcal{D}_{q0}^{(0)}(z)|^2\rangle\rangle. \tag{B3}$$

Employing now the matrix notation introduced in appendix A, the configuration average of Eq. (B3) can be performed explicitly. To be specific, from Eq. (A7) it follows that

$$\begin{aligned}\mathcal{D}_{q0}^{(N)}(z) &= \sum_r\{\left[1 - \tilde{H}^{(N)}(z)\sigma_{imp}^{(N)}(x_i; z)\right]^{-1}\}_{qr} \\ &\times \tilde{H}_{r0}^{(N)}(z),\end{aligned} \tag{B4}$$

which, using the bi-modal probability distribution $p(x_i) = c\delta(x_i) + (1-c)\delta(x_i - 1)$, immediately yields

$$\langle\langle|\mathcal{D}^{(0)}_{q0}(z)|^2\rangle\rangle = \int dx_i\ p(x_i)|\mathcal{D}^{(0)}_{q0}(z)|^2$$
$$= (1-c)|\mathcal{D}^{A,(0)}_{q0}(z)|^2$$
$$+ c|\mathcal{D}^{B,(0)}_{q0}(z)|^2, \qquad \text{(B5)}$$

with the amplitudes $\mathcal{D}^{\lambda,(0)}_{q0}(z)$ satisfying the recursion relations Eq. (A10). Combining Eqs. (B3) and (B5) and setting $z = \omega + i\eta$, we finally obtain Eq. (54).


[1] For an introductory discussion of polarons per se see, e.g., G.D. Mahan, *Many-Particle Physics* (Plenum Press, New York, 1990), Chap. 6.

[2] See, e.g., *Lattice effects in High Temperature Superconductors*, edited by Y. Bar-Yam, T. Egami, J. Mustre de Leon, and A. R. Bishop (World Scientific, Singapore, 1992).

[3] See, e.g., T. A. Tyson *et al.*, Phys. Rev. **B 53**, 13 985 (1996); Y. Yamada *et al.*, Phys. Rev. Lett. **77**, 904 (1996); A. J. Millis, P. B. Littlewood, and B. I. Shraiman, ibid. **74**, 5144 (1995).

[4] See, e.g., D. Mihailović *et al.*, Phys. Rev. **B 42**, 7989 (1990) and references therein.

[5] T. Holstein, Ann. Phys. (N.Y.) **8**, 325 (1959); ibid. 343.

[6] H. de. Raedt and A. Lagendijk, Phys. Rev. B **27**, 6097 (1983).

[7] W. Stephan, Phys. Rev. B **54**, 8981 (1996).

[8] G. Wellein and H. Fehske, Phys. Rev. B **56**, 4513 (1997).

[9] J. Boncă, S. A. Trugman, and I. Batistić, Phys. Rev. B **60**, 1633 (1999).

[10] H. Löwen, Phys. Rev. B **37**, 8661 (1988).

[11] S. Ciuchi, F. de Pasquale, S. Fratini, and D. Feinberg, Phys. Rev. **B 56**, 4494 (1997).

[12] E. V. L. de Mello and J. Ranninger, Phys. Rev. B **55**, 14 872 (1997); J. Ranninger, ibid. **48**, 13 166 (1993).

[13] G. Wellein and H. Fehske, Phys. Rev. B **58**, 6208 (1998).

[14] E.N. Economou and M.H. Cohen, Phys. Rev. B **5**, 2931 (1972).

[15] H. Sumi, J. Phys. Soc. Jpn. **36**, 770 (1974).

[16] H. Miyazaki and E. Hanamura, J. Phys. Soc. Jpn. **50**, 1310 (1981).

[17] H. Miyazaki and E. Hanamura, J. Phys. Soc. Jpn. **51**, 818 (1982); ibid. 828.

[18] S. Abe, J. Phys. Soc. Jpn. **57**, 4029 (1988).

[19] S. Abe, J. Phys. Soc. Jpn. **57**, 4036 (1988); ibid. **59**, 1496 (1990).

[20] D. Paquet and P. Leroux-Hugon, Phys. Rev. B **29**, 593 (1984).

[21] P. Soven, Phys. Rev. **156**, 809 (1967).

[22] B. Velický, S. Kirkpatrick, and H. Ehrenreich, Phys. Rev. **175**, 747 (1968).

[23] B. Velický, Phys. Rev. **184**, 614 (1969).

[24] D. Vollhardt in *Correlated Electron Systems*, edited by V. J. Emery (World Scientific, Singapore).

[25] Th. Pruschke, M. Jarrel, and J. K. Freericks, Adv. Phys. **44**, 187 (1995).

[26] A. Georges, G. Kotliar, W. Krauth, and M.J. Rozenberg, Rev. Mod. Phys. **68**, 13 (1996).

[27] L. Schwartz and H. Ehrenreich, Phys. Rev. B **6**, 2923 (1972).

[28] R. Vlaming and D. Vollhardt, Phys. Rev. B **45**, 4637 (1992).

[29] L. Schwartz and E. Siggia, Phys. Rev. B **5**, 383 (1972).

[30] For more details concerning how to define the various electron-phonon coupling regimes, see, e.g., D. Feinberg, S. Ciuchi, and F. de Pasquale, Int. J. Mod. Phys. B **4**, 1317 (1990).

[31] S. Kirkpatrick, B. Velický, and H. Ehrenreich, Phys. Rev. B **1**, 3250 (1970).

[32] G. Doetsch, *Anleitung zum praktischen Gebrauch der Laplace Transformation und der Z-Transformation* (Oldenburg Verlag, München, 1989).

[33] T. Hotta and Y. Takada, Phys. Rev. Lett. **76**, 3180 (1996).

[34] M. Cini, Phys. Rev. B **29**, 547 (1984).

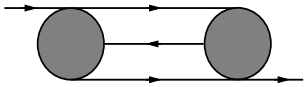

FIG. 1. Schematic representation of a fourth order process contributing to $Q_i^{[2]}$. Atomic T-matrices and effective one-resolvents are, respectively, depicted by solid circles and solid lines. The arrows indicate the order in which the diagram has to be read. The energy arguments are clear from the context.

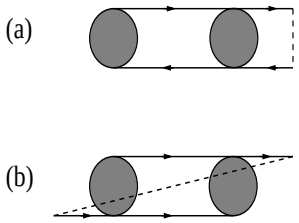


FIG. 2. Schematic representation of the second order (ladder) process contributing to the local DCPA vertex (a) and of the second order (maximally crossed) process neglected within the DCPA (b). The dashed line depicts the operator $O_e$ and solid circles and lines stand, respectively, for atomic T-matrices and effective one-resolvents. The arrows indicate the order in which the diagrams have to be read. The energy arguments are clear from the context.

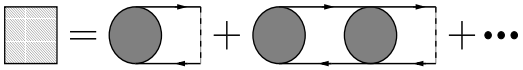

FIG. 3. Schematic representation of Eq. (40). The box on the left hand side denotes the local vertex operator $\Gamma_i$, the dashed line depicts the operator $O_e$, and solid circles and lines stand, respectively, for atomic T-matrices and effective one-resolvents. The arrows indicate the order in which the diagram has to be read. The energy arguments are clear from the context.

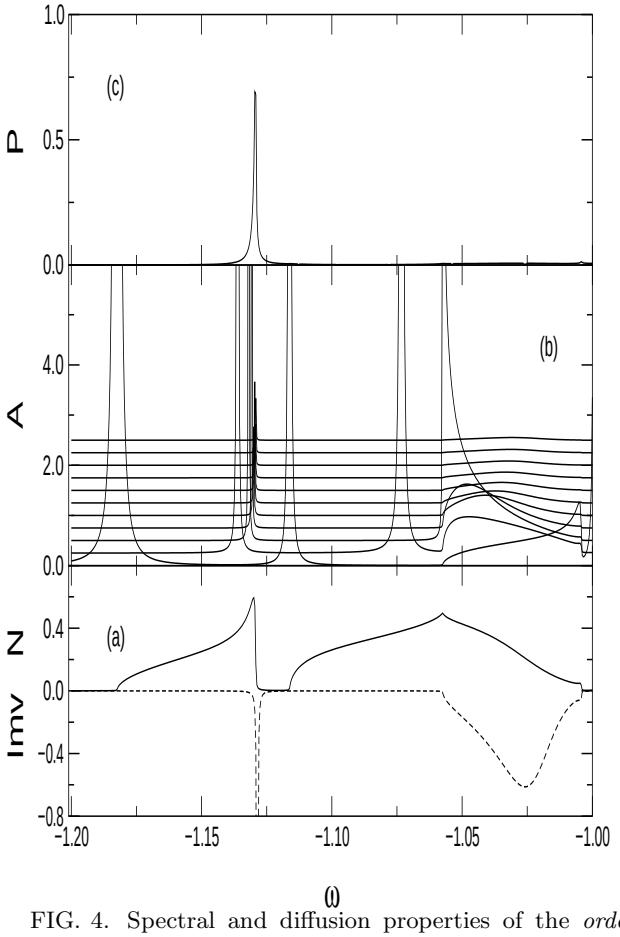


FIG. 4. Spectral and diffusion properties of the *ordered* Holstein model in the vicinity of the first polaronic subband for $\lambda = 1.96$, $\alpha = 2.8$ [see Table I], and $\eta = 10^{-4}$. (a) Density of states $N(\omega)$ (solid line) and imaginary part of the coherent potential $Imv(\omega)$ (dashed line). (b) Spectral function $A(\omega, \epsilon_{\vec{k}})$ with $\epsilon_{\vec{k}}$ ranging from $\epsilon_{\vec{k}} = -1$ to $\epsilon_{\vec{k}} = 1$ (bottom to top) in steps of $\Delta\epsilon_{\vec{k}} = 0.2$. For clarity the spectral functions corresponding to different $\epsilon_{\vec{k}}$ are artificially shifted along the vertical axis. (c) Spectrally resolved return probability $P(\omega, \eta)$.

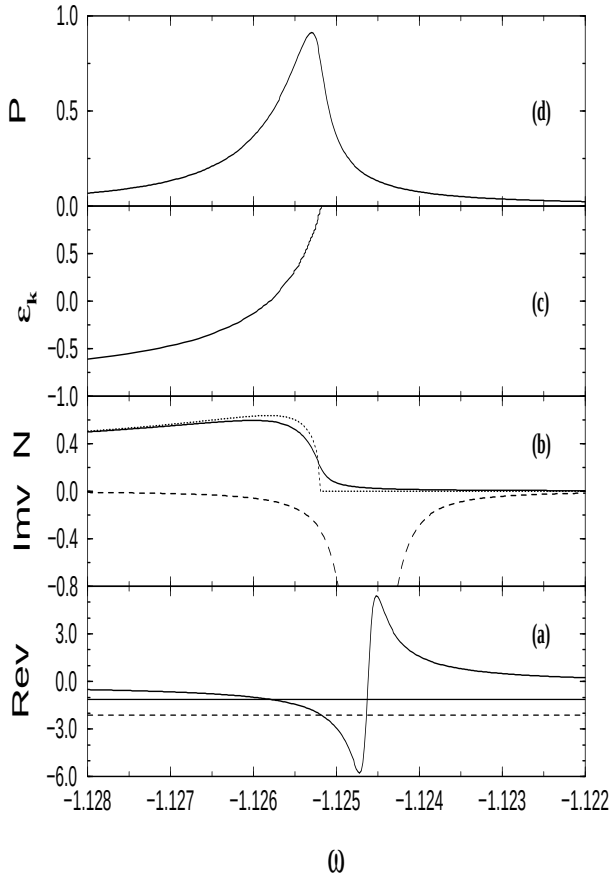


FIG. 5. Blow-up of Fig. 4 in the immediate vicinity of the high-energy edge of the lowest polaronic subband. (a) Real part of the coherent potential $Rev(\omega)$ for $\eta = 10^{-4}$ (thick solid line). The intersections (below $\omega = -1.125$) with the thin solid and dashed lines determine, respectively, the position of the maximum of the subband density of states ($\omega_m$) and the position of the high-energy edge ($\omega_h$). (b) Density of states for $\eta = 10^{-4}$ (solid line) and $\eta = 10^{-8}$ (dotted line). The dashed line depicts the imaginary part of the coherent potential $Imv(\omega)$ for $\eta = 10^{-4}$. (c) The poles of the spectral function $\omega(\epsilon_{\vec{k}})$. Here we plot $\epsilon_{\vec{k}}$ vs. $\omega$. (d) Spectrally resolved return probability $P(\omega, \eta)$ for $\eta = 10^{-4}$.

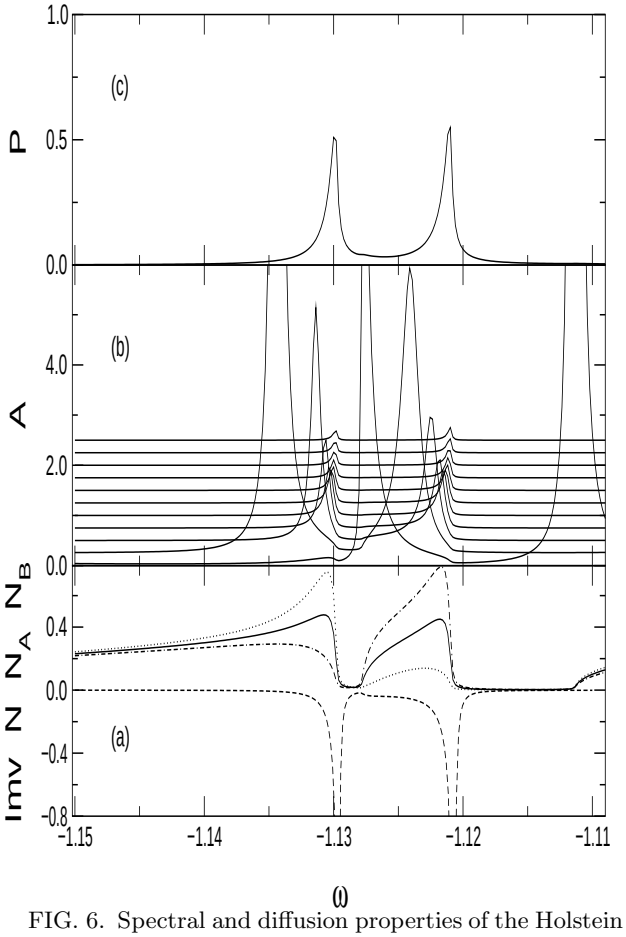


FIG. 6. Spectral and diffusion properties of the Holstein alloy in the vicinity of the high-energy edge of the first polaronic subband for $c = 0.5$ and $\delta = -0.01$. The polaron parameters are $\lambda = 1.96$ and $\alpha = 2.8$ [see Table I] and $\eta = 10^{-4}$. (a) Density of states $N(\omega)$ (solid line), component density of states $N_A(\omega)$ (dotted line) and $N_B(\omega)$ (dot-dashed line), and imaginary part of the coherent potential $Imv(\omega)$ (dashed line). (b) Spectral function $A(\omega, \epsilon_{\vec{k}})$ with $\epsilon_{\vec{k}}$ ranging from $\epsilon_{\vec{k}} = -1$ to $\epsilon_{\vec{k}} = 1$ (bottom to top) in steps of $\Delta\epsilon_{\vec{k}} = 0.2$. For clarity the spectral functions corresponding to different $\epsilon_{\vec{k}}$ are artificially shifted along the vertical axis. (c) Spectrally resolved return probability $P(\omega, \eta)$.

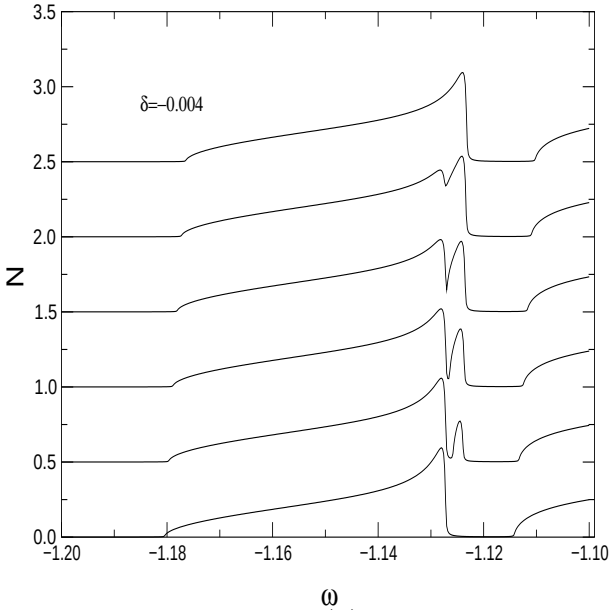


FIG. 7. Density of states $N(\omega)$ for the Holstein alloy in the vicinity of the first polaronic subband. The polaron parameters are $\lambda = 1.96$ and $\alpha = 2.8$ [see Table I] and $\eta = 10^{-4}$. The scattering strength $\delta = -0.004$ and the concentration of the B atoms varies from $c = 0.0$ (bottom) to $c = 1.0$ (top) in steps of $\Delta c = 0.2$. For clarity the density of states corresponding to different concentrations are artificially shifted along the vertical axis.

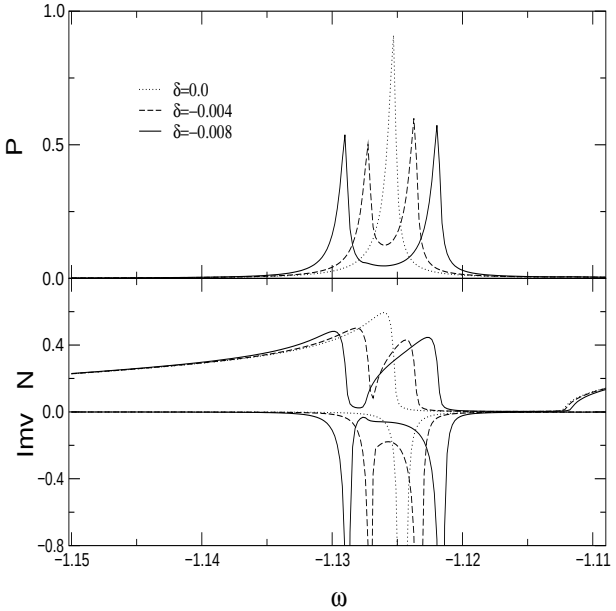


FIG. 8. The lower panel shows the density of states $N(\omega)$ and the imaginary part of the coherent potential $Imv(\omega)$ for the Holstein alloy in the vicinity of the high-energy edge of the first polaronic subband for $c = 0.5$ and three different values of the scattering strength $\delta$. The polaron parameters are $\lambda = 1.96$ and $\alpha = 2.8$ [see Table I] and $\eta = 10^{-4}$. The corresponding spectrally resolved return probabilities $P(\omega, \eta)$ are given in the upper panel.

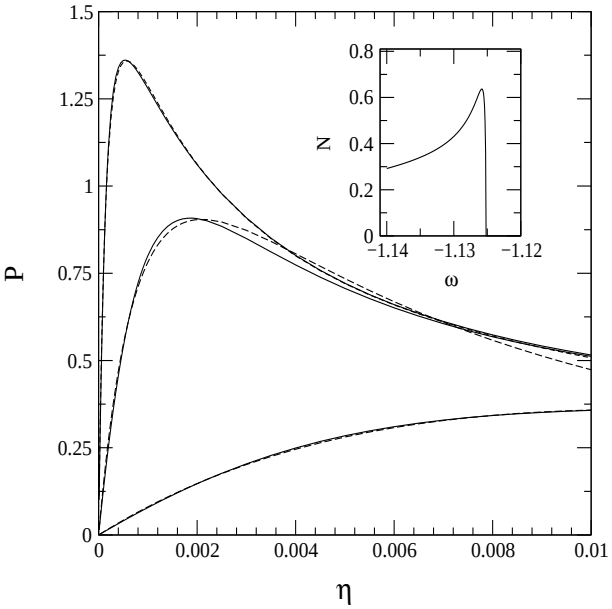


FIG. 9. $\eta-$asymptotics of the spectrally resolved return probability $P(\omega, \eta)$ for the ordered Holstein model. The polaron parameters are $\lambda = 1.96$ and $\alpha = 2.8$ [see Table I]. The three sets of curves correspond to three energies: $\omega = -1.135, -1.127$, and $-1.12549$ (from bottom to top). Solid [dashes] lines depict the numerical data [asymptotic expansion given in Eq. (60)]. The corresponding density of states for $\eta = 10^{-8}$ is shown in the inset.

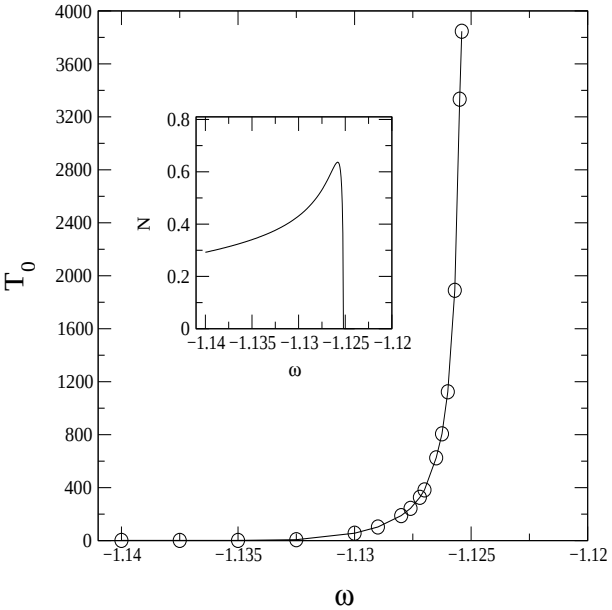


FIG. 10. Spectrally resolved delocalization time $T_0(\omega)$ for the ordered Holstein model in the vicinity of the high energy edge of the first polaronic subband. The polaron parameters are $\lambda = 1.96$ and $\alpha = 2.8$ [see Table I]. The inset shows the density of states for $\eta = 10^{-8}$. Note, the data for $T_0(\omega)$ are for energies below the $\eta \to 0$ high-energy edge.

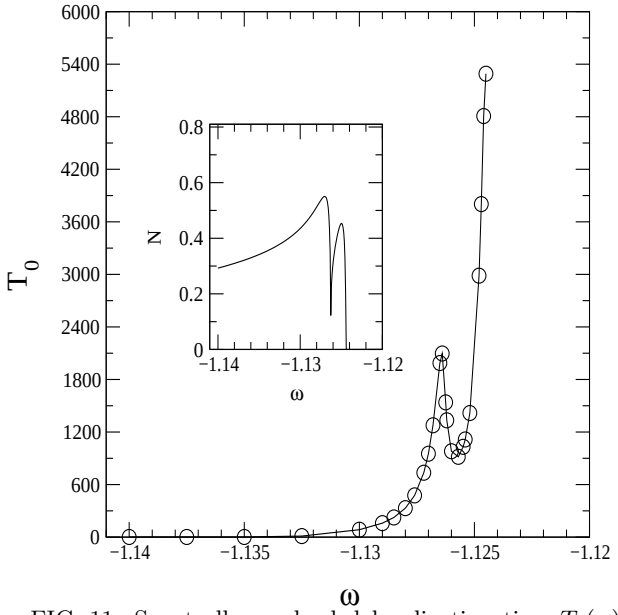


FIG. 11. Spectrally resolved delocalization time $T_0(\omega)$ for the Holstein alloy in the vicinity of the high energy edge of the first polaronic subband for $c = 0.5$ and $\delta = -0.002$. The polaron parameters are $\lambda = 1.96$ and $\alpha = 2.8$ [see Table I]. The inset shows the density of states for $\eta = 10^{-8}$. Note, the data for $T_0(\omega)$ are for energies below the $\eta \to 0$ high-energy edge.

TABLE I. Polaron model parameters (in units of $2J$)

| J | $\Omega$ | g | $\lambda = 2g^2/\Omega$ | $\alpha = g/\Omega$ |
|---|---|---|---|---|
| 0.5 | 0.125 | 0.35 | 1.96 | 2.8 |